EUROPEAN ORGANIZATION FOR NUCLEAR RESEARCH

CERN-EP/89-14
January 19th, 1989

Measurement of the Z_1^3-contribution to the stopping power using MeV protons and antiprotons - the Barkas effect

L.H. Andersen, P.Hvelplund, H.Knudsen, S.P.Møller,
J.O.P.Pedersen, and E.Uggerhøj
Institute of Physics, University of Aarhus
DK-8000 Aarhus C, Denmark

K.Elsener
CERN, CH-1211 Geneva 23, Switzerland

E.Morenzoni
PSI, CH-5234 Villigen, Switzerland

Abstract

The stopping power of silicon has been measured for protons and antiprotons with energies between 3.5 and 0.5 MeV. The stopping power for antiprotons is found to be 3-19% lower than for equivelocity protons over the energy range investigated. The "Z_1^3-contribution" to the stopping power (the Barkas effect) is deduced by comparing the stopping power for protons and antiprotons. These data constitute the first clear evidence of a significant close-collision contribution to the Barkas effect.

(Submitted to Phys.Rev.Letters)

PACS No.: 29.70.Gn, 34.50.Bw, 61.80.Mk

The theory of energy loss of fast charged particles in matter is based on the calculations by Bethe[1], who derived the stopping power in the first Born approximation. Hence the Bethe result is proportional to the projectile charge squared, Z_1^2. It was thus a surprise when Barkas et al.[2] found, that the range of negative pions was longer than that of positive pions of equal momentum, and the effect was first attributed to a mass difference. Later Barkas et al.[3] suggested that the effect was due to a difference in the stopping power stemming from the opposite charge of the particles. The reduction in the stopping power, responsible for the longer range, of negative particles as compared to their positively charged antiparticles was later investigated with both sigma-hyperons[3], pions[4] and muons[5], but these measurements all suffer from the poor quality of the low-velocity particle/antiparticle beams used.

The so-called Barkas effect was interpreted as a polarization effect in the stopping material depending on the charge of the projectile, appearing as the next term (proportional to Z_1^3) in the implied Born expansion of the energy loss. The Barkas correction, which is a classical effect, was first calculated by Ashley, Ritchie and Brandt[6] using a classical perturbation calculation for a harmonic oscillator. The effect originates in the non-negligible displacement of the atomic electron during the collision, which was included to first order in the calculation. Their calculation only applies for distant collisions, but the authors assert that the close collisions are essentially those of free particles, giving an exact Z_1^2-dependence. The minimum impact parameter for distant collisions, of major importance for the result, has been used as an adjustable parameter to fit experimental results. At the same time Jackson and McCarthy[7] performed a similar, but relativistic, calculation arriving at the same conclusions, but they chose the minimum impact parameter as the radius of the harmonic oscillator in question. Subsequently Lindhard[8] argued that there

is an equally important contribution to the Z_1^3-term from the close collisions, which are not Coulomb-like due to dynamical screening of the projectile charge by the atomic electrons. The influence of the particle field is adiabatic for electrons outside a sphere of radius v/ω, where v is the projectile velocity and ω the oscillation frequency of the electron. Consequently positive/negative particles will have a smaller/larger velocity during the central part of the collision than in a collision between free particles, leading to larger energy transfers for positive particles than for negative in the close collisions. This contribution was estimated to be comparable to the distant-collision contribution as calculated by Jackson and McCarthy. Many other calculations of the Barkas effect have appeared, but the principal disagreement is still on the question, whether or not the close collisions contribute to the Barkas effect, resulting in a discrepancy of roughly a factor of two between different estimates of the effect.

Deviations from a strict Z_1^2-dependence of the stopping power also emerge when comparing the stopping power for protons and alpha particles[9]. However, to extract the Z_1^3-correction, it is also necessary to include data for particles of charge other than +1 and +2, for example Li-nuclei[10], since the Z_1^4-term in the Born expansion of the stopping power is non-negligible for projectile velocities of a few atomic units[8]. Part of the Z_1^4-contribution is the Bloch-term[8], marking the transition to the classical scattering regime. Furthermore the analysis is somewhat hampered by electron capture of the Li nuclei, and it is not possible experimentally to discern whether the close collisions contribute to the Barkas term[11]. For recent reviews of the experimental and theoretical situation, see refs. 11 and 12.

With the advent of LEAR at CERN, high-quality beams of antiprotons at low energy became available, making an accurate comparison of stopping powers for antiprotons and protons feasible. The present experiment was performed with the 105.5 MeV/c (5.91 MeV kinetic energy) LEAR beam, which

had an intensity of ~10^4 sec^{-1} and a momentum spread of ~10^{-3}. The beam exits the LEAR ultra-high vacuum system through a ~100 μm Be window, passes through ~2 cm of air and enters the experimental vacuum chamber through a 22 μm mylar foil. Next, the beam traverses a 100 μm scintillator (start), which together with another scintillator (stop) ~1m downstream, is used to measure the time-of-flight (TOF) of the beam particles. Lower proton and antiproton energies were obtained by inserting various aluminum degrader foils in the air between the two vacuum systems. For each degrader, TOF-spectra were recorded with the stop scintillator at two positions, with an accurately determined distance of 0.5 m. The time resolution of the system was 1.0 ns (RMS) corresponding to an energy resolution of 10% at 3 MeV and 4% at 0.6 MeV, but the peak of the distribution, used in the energy-determination, was determined much better, leading to an energy uncertainty of less than 1%.

The energy loss of the particles was measured as the energy deposited in two thin transmission silicon detectors, 6.9 and 2.9 μm thick, respectively. The energy resolution of these detectors was 6.2 and 7.8 keV (RMS), which is less than the energy straggling in the detectors. For beams degraded to less than 2 MeV, the energy straggling from the degrader dominates over the straggling in the silicon detector. There is a difference between the energy deposited in the Si-detector, which is measured, and the energy lost by the particles, which is calculated. This difference is mainly caused by escape of δ rays, but as discussed in ref. 10, the corrections amount to less than a few times 10^{-3}. Since the Si-detector is a single crystal, channeling may change the energy loss. By tilting the detector slightly around perpendicular beam incidence, it was assured that the energy-loss spectra were without detectable influence of channeling. A channeling effect was seen for protons, but not for antiprotons. To exclude the edge of the detector, the signals from the 10 mm^2 transmission detectors were gated with a 7 mm^2 thick Si-detector mounted behind the ΔE-detector.

An electronic pulser and a polonium α source assured stability of the amplifier system.

As an example of an energy-loss spectrum, fig.1 shows a spectrum from the 6.9 μm ΔE-detector for 3.01 MeV incident antiprotons. The energy-loss distribution is slightly asymmetric with a small high-energy tail. A small background from annihilation products is visible. The distribution is a Vavilov distribution since the parameter characterizing the distribution function, $\kappa = \xi/E_{max}$ is of the order of unity. Here $\xi = 2\pi e^4 \Delta x N Z_2/mv^2$ and the maximum energy transfer $E_{max} = 2\,mv^2$, where Δx is the target thickness, N the target density, Z_2 the target atomic number, v the projectile velocity, and m and e the electron mass and charge, respectively. The tail in the energy-loss distribution is included in the extraction of the average energy loss.

The stopping power is determined as the energy loss divided by the target thickness, $\Delta E/\Delta x$, at the average energy $\bar{E} = E_0 - \Delta E/2$, where E_0 is the incident particle energy. Multiple scattering can be neglected, as the average path length of the particles in the target is less than 0.2% larger than the actual target thickness. To calibrate the ΔE-detector, proton stopping powers were measured at a few energies. The proton reference beams of 1.5 to 3.5 MeV were also obtained by degradation of a 105.5 MeV/c beam from LEAR. The calibration constant was found by requiring the measured proton stopping powers to agree with the recommended values by Andersen and Ziegler[13]. The measured stopping powers for protons and antiprotons for the two ΔE-detectors are shown in fig.2. We observe that the measured proton stopping power follows the full-drawn curve (from ref.13) to better than 1%, giving confidence into the method used. It is also seen, that the measured antiproton stopping power is lower than that of protons, as expected. The difference is 3% at 3.01 MeV and 19% at 0.538 MeV. Finally, there is consistency between the measurements with the two ΔE-detectors.

The main feature of fig.2 is, however, the uninteresting $1/v^2$ depen-

dence of the stopping power. The Bethe result for the stopping power is given by

$$-\frac{dE}{dx} = \frac{4\pi e^4 NZ_2}{mv^2} Z_1^2 L_0 \quad , \tag{1}$$

where the Bethe stopping function L_0, which is independent of Z_1, may be written

$$L_0 = \ln\left(\frac{2mv^2}{I(1-\beta^2)}\right) - \beta^2 - \frac{C}{Z_2} \quad , \tag{2}$$

$\beta=v/c$ being the projectile velocity relative to the velocity of light c, I the mean ionization potential and C/Z_2 the so-called shell corrections.

Formally one may generalize the above stopping power formula, eq. (1), by including higher order Z_1-terms in the stopping function

$$L = L_0 + Z_1 L_1 + Z_1^2 L_2 + \ldots \quad , \tag{3}$$

where L_1 and L_2 are the Z_1-independent coefficients of the Z_1^3- and Z_1^4-terms in the stopping power, and where higher-order terms are omitted. The first term L_0 is the Bethe stopping function, eq.(2), $Z_1 L_1$ the Barkas term and $Z_1^2 L_2$ includes the Bloch correction. To elucidate the interesting part of the measured stopping powers, we plot in fig. 3 the so-called reduced stopping power X, which is the stopping power reduced for the trivial factors

$$X = \ln\left(\frac{2mv^2}{I(1-\beta^2)}\right) - \beta^2 - \frac{mv^2}{4\pi e^4 NZ_2 Z_1^2}\left(-\frac{dE}{dx}\right) = \ln\left(\frac{2mv^2}{I(1-\beta^2)}\right) - \beta^2 - L. \tag{4}$$

We have used the value I = 165 eV (ref. 13). The theoretical reduced stopping power is now given as

$$X_{theor} = \frac{C}{Z_2} - Z_1 L_1 - Z_1^2 L_2 . \qquad (5)$$

The two curves in fig. 3 represent the reduced stopping power from ref. 13 (protons) and the same stopping power corrected for the Lindhard Z_1^3-term[8] corresponding to twice the Jackson and McCarthy value[7]. The difference in the measured stopping for protons and antiprotons is now clearly visible. The error bars correspond to ±1% on the stopping power, which is the estimated uncertainty. The proton measurements agree with the recommended curve (ref. 13) within the uncertainty. The measured antiproton stopping powers are in reasonable agreement with the Lindhard result, especially for the high-energy points.

Finally, in fig. 4 we have extracted the Barkas term L_1 from the data, using the stopping power from ref. 13 for protons. The results are here plotted as a function of the velocity in units of the Bohr velocity $v_0 = \alpha c$, $\alpha = e^2/\hbar c$ being the fine-structure constant. The error bars stem from the ±1% uncertainty on the stopping-power measurement. The full-drawn curve is the Jackson and McCarthy result (ref. 7) and the dashed line is twice the result of this calculation as suggested by Lindhard[8]. The measurements coincide with the latter curve for the higher velocities, but there seems to be a tendency for the measured points to fall slightly below the curve for the lower velocities. In particular, the calculated velocity-dependence of L_1 essentially reproduces the observed one ($\propto v^{-2}$). Consequently the measured Barkas term is around a factor of two larger than that calculated by Jackson and McCarthy for the distant collisions only, and in close agreement with the estimate of the Barkas term by Lindhard[8] with roughly equal contributions from close and distant collisions.

In ref. 14, some of us observed an increased double-ionization cross section for antiprotons in noble gases as compared to proton impact. It was demonstrated, that such an effect, which is not included in any calcula-

tions of stopping power, leads to a non-negligible contribution to the Barkas effect of opposite sign than polarization effects. This effect could also play a role for solids, such as silicon.

Earlier experiments[4,5,10], on other targets than silicon, have shown indications of a Z_1^3-contribution to the stopping power of slightly larger magnitude than reported here, but experimental uncertainties or uncertainties in the interpretation of the data have prevented a clear estimate of the L_1-term.

The present measurements of the Z_1^3-correction to the stopping power allows for the first time an unambiguous extraction of the shell corrections from stopping power measurements. In this connection there is an interest in extending the present measurements to lower antiproton velocities and other targets. The simplicity and accuracy of the present method in obtaining relative stopping powers for antiprotons and protons relies on the target being a semiconductor detector. For other targets, the antiproton energy would have to be measured before and after the target with spectrometric techniques. For energies lower than 0.5 MeV, this would with the present minimum momentum of 105 MeV/c from LEAR have to be done on an event-by-event basis due to the large straggling from the degrader.

References

1. H.A. Bethe, Ann.Phys.(Leipzig) 5, 325 (1930);
   U. Fano, Ann.Rev.Nucl.Sci. 13, 1 (1963)
2. W.H. Barkas, W. Birnbaum and F.M. Smith, Phys.Rev. 101, 778 (1956)
3. W.H. Barkas, N.J. Dyer and H.H. Heckman, Phys.Rev.Lett. 11, 26 (1963)
4. H.H. Heckman and P.J. Lindstrom, Phys.Rev.Lett. 22, 871 (1969)
5. W.Wilhelm, H.Daniel and F.J. Hartmann, Phys.Lett. 98B, 33 (1981)
6. J.C.Ashley, R.H.Ritchie, and W.Brandt Phys.Rev. B 5, 2393 (1972);
   ibid A 8, 2402 (1973)
7. J.D. Jackson and R.L.McCarthy, Phys.Rev. B 6, 4131 (1972)
8. J. Lindhard, Nucl.Instrum.Methods 132, 1 (1976)
9. H.H. Andersen, H. Simonsen and H. Sørensen, Nucl.Phys.A 125, 171 (1969)
10. H.H. Andersen, J.F. Bak, H.Knudsen and B.R. Nielsen, Phys.Rev.A 16, 1929 (1977)
11. H.H. Andersen in, "Semiclassical Descriptions of Atomic and Nuclear Collisions", J. Bang et al., eds., Elsevier Sci.Publ. (1985), p.409
12. G.Basbas, Nucl.Instrum.Methods B 4, 227 (1984)
13. H.H. Andersen and J.F. Ziegler, "Hydrogen Stopping Powers and Ranges in All Alements", Pergamon, New York, 1977
14. L.H. Andersen, P. Hvelplund, H. Knudsen, S.P. Møller, A.H.Sørensen, K.Elsener, K.-G. Rensfelt and E. Uggerhøj, Phys.Rev.A 36, 3612 (1987)

Figure Captions

Fig. 1: Energy-loss spectrum for 3.01 MeV antiprotons traversing the 6.9 μm Si detector.

Fig. 2: Measured stopping power of Si for protons and antiprotons from this work. The solid curve is the recommended stopping power for protons from ref. 13.

Fig. 3: Reduced stopping power, eq.(4), of Si for protons and antiprotons. The solid curves show the reduced stopping power from ref. 13, the upper curve including the Barkas effect corresponding to twice the Jackson-McCarthy result[7].

Fig. 4: The Z_1^3-contribution, L_1, to the stopping power extracted from the measurements. The full-drawn and the dashed curve correspond to the Jackson-McCarthy result and twice this value, respectively.

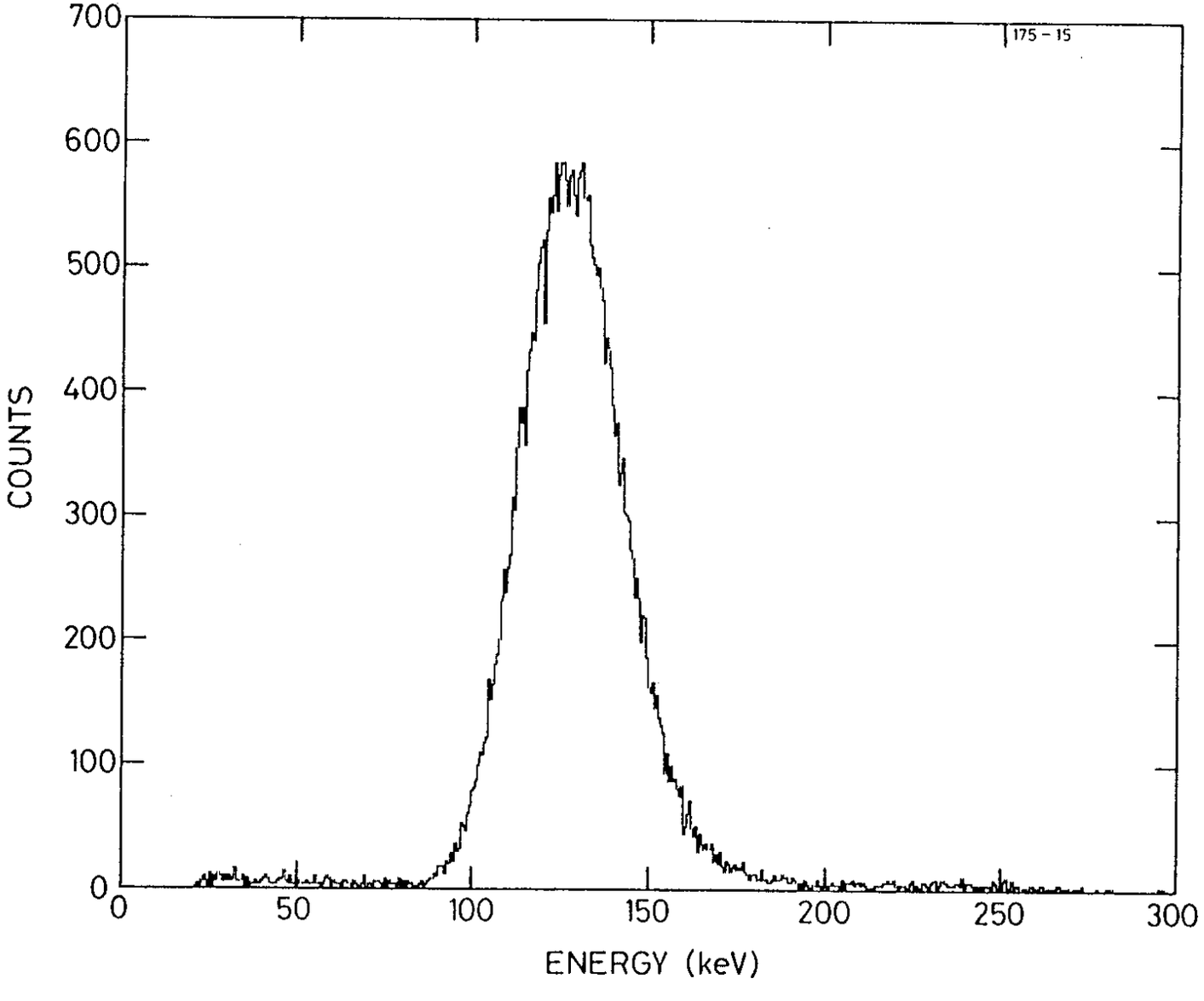
175 - 15
700
600
500
400
300
200
100
0
COUNTS
0
50
100
150
200
250
300
ENERGY (keV)

Fig. 1

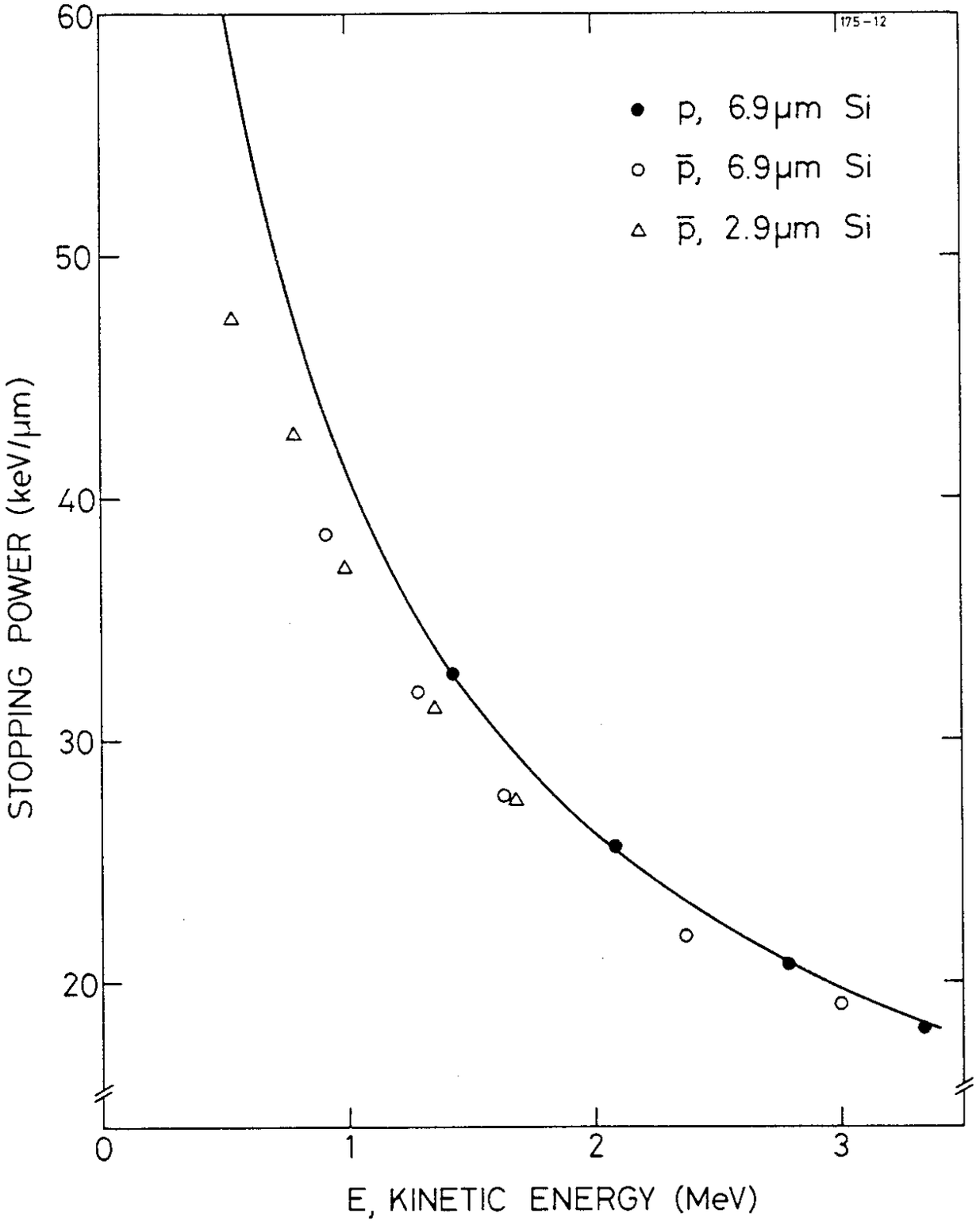
175-12
p, 6.9μm Si
p̄, 6.9μm Si
p̄, 2.9μm Si
STOPPING POWER (keV/μm)
60
50
40
30
20
0
1
2
3
E, KINETIC ENERGY (MeV)

Fig. 2

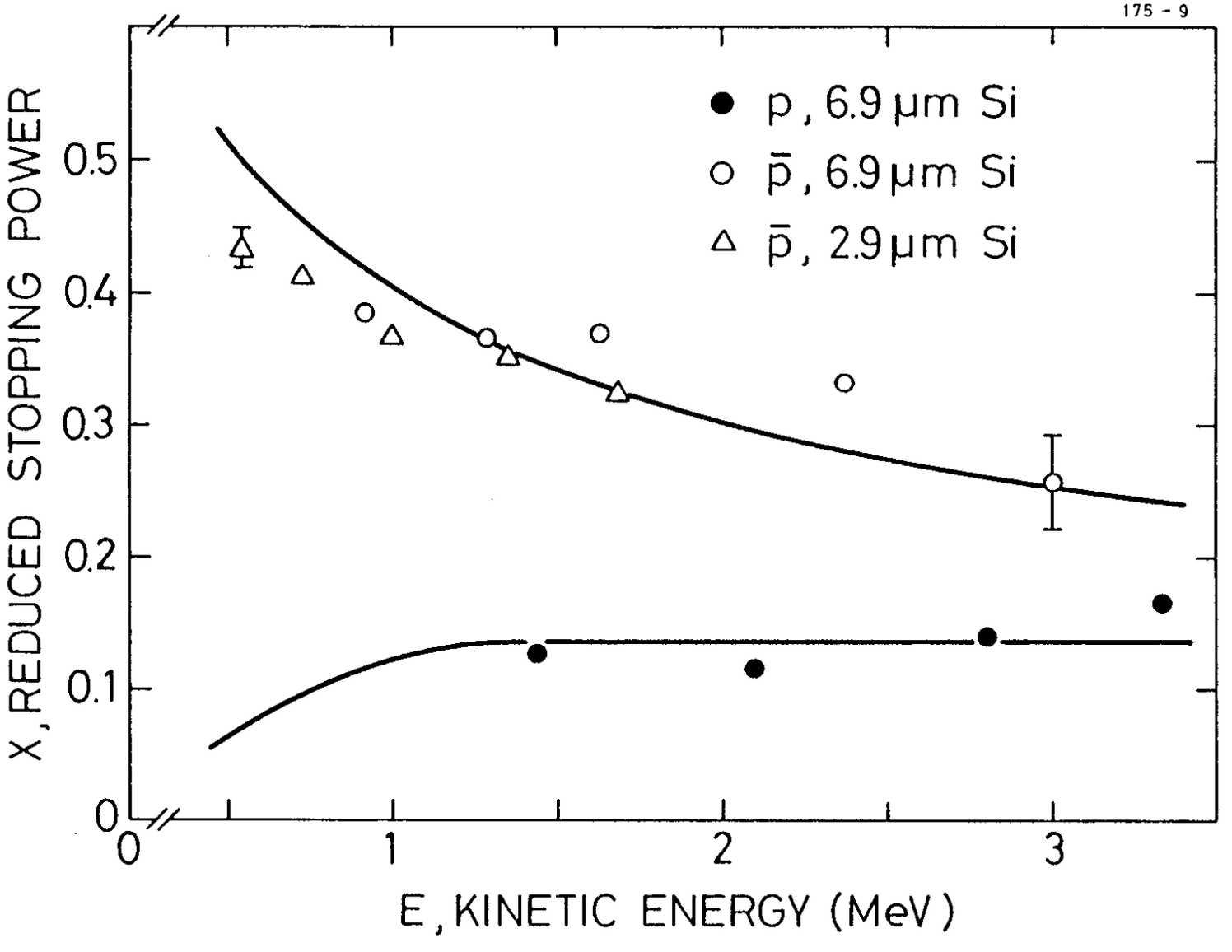
175 - 9
p , 6.9 μm Si
p̄ , 6.9 μm Si
p̄ , 2.9 μm Si
X, REDUCED STOPPING POWER
0
0.1
0.2
0.3
0.4
0.5
0
1
2
3
E, KINETIC ENERGY (MeV)

Fig. 3

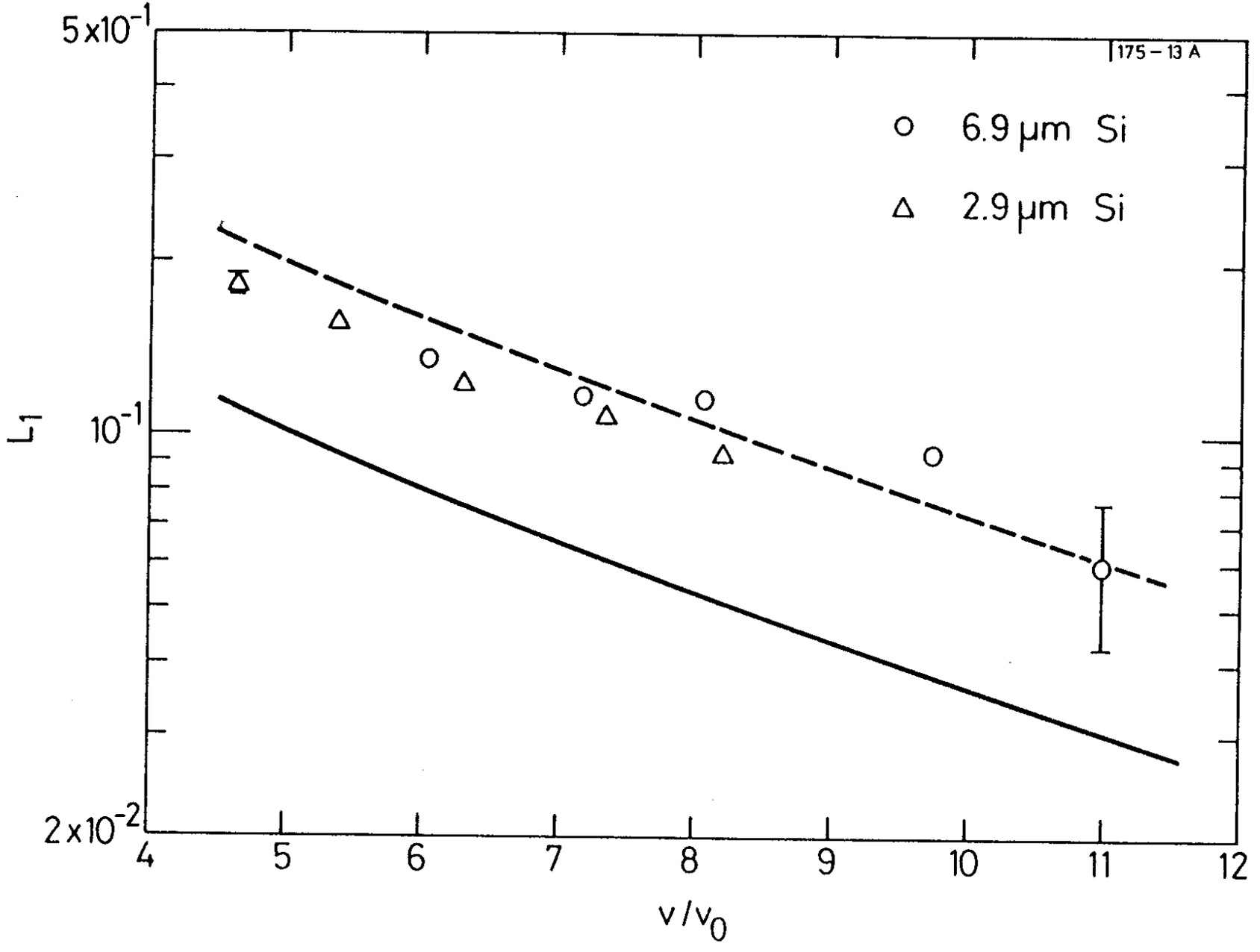
175 – 13 A
6.9 µm Si
2.9 µm Si
5×10^{-1}
10^{-1}
2×10^{-2}
L_1
4
5
6
7
8
9
10
11
12
v/v_0

Fig. 4